

Article

# Amplification of Wave Groups in the Forced Nonlinear Schrödinger Equation

Montri Maleewong <sup>1,\*</sup>  and Roger H. J. Grimshaw <sup>2,\*</sup>

<sup>1</sup> Department of Mathematics, Faculty of Science, Kasetsart University, Bangkok 10900, Thailand

<sup>2</sup> Department of Mathematics, University College London, London WC1E 6BT, UK

\* Correspondence: montri.m@ku.th (M.M.); rhjgrimshaw@gmail.com (R.H.J.G.)

**Abstract:** In many physical contexts, notably including deep-water waves, modulation instability in one space dimension is often studied by using the nonlinear Schrödinger equation. The principal solutions of interest are solitons and breathers which are adopted as models of wave packets. The Peregrine breather in particular is often invoked as a model of a rogue wave. In this paper, we add a linear growth term to the nonlinear Schrödinger equation to model the amplification of propagating wave groups. This is motivated by an application to wind-generated water waves, but this forced nonlinear Schrödinger equation potentially has much wider applicability. We describe a series of numerical simulations which in the absence of the forcing term would generate solitons and/or breathers. We find that overall the effect of the forcing term is to favour the generation of solitons with amplitudes growing at twice the linear growth rate over the generation of breathers.

**Keywords:** wind waves; breathers; soliton; nonlinear Schrodinger; rogue; modulation instability



**Citation:** Maleewong, M.; Grimshaw, R.H.J. Amplification of Wave Groups in the Forced Nonlinear Schrödinger Equation. *Fluids* **2022**, *7*, 233. <https://doi.org/10.3390/fluids7070233>

Academic Editors: Mehrdad Massoudi and Xavier Carton

Received: 14 June 2022

Accepted: 5 July 2022

Published: 8 July 2022

**Publisher's Note:** MDPI stays neutral with regard to jurisdictional claims in published maps and institutional affiliations.



**Copyright:** © 2022 by the authors. Licensee MDPI, Basel, Switzerland. This article is an open access article distributed under the terms and conditions of the Creative Commons Attribution (CC BY) license (<https://creativecommons.org/licenses/by/4.0/>).

## 1. Introduction

It is well known that modulation instability, that is, the exponential growth of long wave perturbations to a periodic plane wave, leads to the formation of nonlinear wave packets, and sometimes to rogue waves. This process is often modelled by the nonlinear Schrödinger equation (NLS), and then the nonlinear wave packets can be represented by the soliton and breather solutions of the NLS, while rogue waves are often modelled by the Peregrine breather (see for instance Kharif et al. [1], Osborne [2], Grimshaw and Tovbis [3]) in the deep-water wave context. The process occurs in many other physical contexts (see Grimshaw et al. [4], Chow et al. [5]) for internal wave applications, and the related articles in that special issue for other cases. In this paper, we develop the formulation in the water wave context to be specific, but the outcome can be applied to many other physical contexts.

In the pioneering work of Benney and Newell [6], Zakharov [7], Hasimoto and Ono [8], the NLS equation for water waves is derived by using a multi-scale asymptotic expansion, in which the leading order nonlinear terms are balanced by weak linear dispersion around the dominant carrier wavenumber of the wave packet (see the review by Grimshaw [9]). A wave packet in one horizontal space dimension is given by

$$\zeta = \delta A(X, T) \exp(i\theta) + \text{c.c.} + \dots, \quad (1)$$

$$\text{where } \theta = kx - \omega(k)t, X = \delta(x - c_g t), T = \delta^2 t. \quad (2)$$

$$\omega^2(k) = \frac{g}{h} q \sigma, \quad c_g = \omega_k = \frac{\omega}{2k} \left\{ 1 + \frac{q}{\sigma} (1 - \sigma^2) \right\}, \quad q = kh, \quad \sigma = \tanh q. \quad (3)$$

Here  $\zeta(x, t)$  is the water surface elevation above the undisturbed depth  $h$ , and  $k$  is the carrier wavenumber, while the wave frequency  $\omega(k)$  satisfies the linear dispersion relation.  $A(x, t)$  is the slowly varying wave amplitude, and at the leading order the wave packet moves with the group velocity  $c_g = \omega_k$ .  $\delta, 0 < \delta \ll 1$  is a small, dimensionless parameter

measuring the wave amplitude and dispersion about the dominant wavenumber  $k$ . The leading order omitted terms in (1) are  $O(\delta^2)$  second harmonic and mean flow terms.

A multi-scale asymptotic expansion in  $\delta$  in which the linear dispersive effects are scaled to balance the leading order nonlinear effects leads to the NLS equation,

$$iA_T + \lambda A_{XX} + \mu |A|^2 A = 0, \quad \lambda = \frac{c_g k}{2}. \tag{4}$$

The coefficient  $\mu$  of the nonlinear term is given by

$$\mu = -\frac{k^2 \omega}{4\sigma^4} (9\sigma^4 - 10\sigma^2 + 9) + \frac{\omega^3}{2\sigma^3 (gh - c_g^2)} (2\sigma(3 - \sigma^2) + 3q(1 - \sigma^2)^2). \tag{5}$$

Note that due to the balance of terms, the small parameter  $\delta$  can be omitted in (4). In deep water ( $q \rightarrow \infty$ ), the second term vanishes, and the coefficient  $\mu \rightarrow -2\omega k^2 < 0$ . In general,  $\mu < 0 (> 0)$  according as  $q > q_c (q < q_c)$ , where  $q_c = 1.363$ . Modulation instability occurs when  $\mu\lambda > 0$ . For water waves  $\lambda < 0$  and so modulation instability occurs for waves in deep water when  $\mu < 0, q > q_c$ . Similar expansions apply in many other physical systems, again leading to the NLS Equation (4). The main difference is the linear dispersion relation (3) and in the expressions for the coefficients  $\lambda, \mu$  (see Grimshaw [9], Akhmediev and Pelinovsky [10] for instance). We note that in this water wave context, the wave amplitude from (1) is  $2\delta A$  and is required to be small since  $\delta \ll 1$  but  $\delta$  itself does not appear explicitly in (4).

In this paper, we are concerned with the effect of forcing on modulation instability. We model this by extending the NLS Equation (4) to a forced NLS equation (fNLS) by the addition of a linear forcing term (see for instance Leblanc [11], Touboul et al. [12], Montalvo et al. [13], Brunetti et al. [14], Slunyaev et al. [15], Grimshaw [16,17,18]) in the wind wave context,

$$iA_T + \lambda A_{XX} + \mu |A|^2 A = i\Delta A. \tag{6}$$

The forcing is modelled by the linear growth rate term with coefficient  $\Delta > 0$ . Various expressions can be found in the literature, the most well-known being that originally derived by Miles [19] and subsequently adapted and modified in various ways (see for instance Grimshaw [16], Miles [20], Morland and Saffman [21], Janssen [22], Stiassnie et al. [23], Sajjadi et al. [24], Zakharov et al. [25]). Here our concern is with the effect of  $\Delta$  on modulation instability and wave packet, or breather, formation. The effect of forcing on modulation instability has been examined in the present one space-dimension framework for deep water waves by Leblanc [11], Touboul et al. [12], Brunetti et al. [14], Slunyaev et al. [15], Grimshaw [16]. Here we extend these studies, which were mostly concerned with the evolution of wave spectra, by focusing on the development of wave packets through comprehensive numerical simulations of the fNLS Equation (6). Validation of the NLS simulations concerning modulation instability and the formation of rogue waves in the water wave tank, is described by Chabchoub et al. [26]. A similar study of the Peregrine breather over zero background was recently given by Chabchoub et al. [27]. Some numerical simulations based on a higher order NLS equation were conducted and compared with experimental studies to validate the numerical simulations of modulation instability and rogue waves (see Onorato et al. [28] and León and Osborne [29]). Here we have performed numerical simulations by adding a forcing term to model the formations of solitons and breathers under external forcing. The formulation of the problem is presented in Section 2. In Section 3, we present these numerical simulations and some accompanying analysis. We conclude in Section 4.

## 2. Formulation

We consider the case when there is modulation instability, so that  $\mu < 0, \lambda < 0 (q > q_c)$ . Then fNLS (6) can be expressed in canonical form

$$i\epsilon Q_T + \epsilon^2 Q_{XX} + 2|Q|^2 Q = i\Delta Q. \tag{7}$$

This canonical form is achieved through the change of variables

$$Q = \left\{ \frac{|\mu|}{2} \right\}^{1/2} \bar{A}, \quad \tilde{X} = \frac{\epsilon}{|\lambda|^{1/2}} X, \quad \tilde{T} = \epsilon T. \tag{8}$$

Here we have introduced the free parameter  $\epsilon$  as it is useful to represent the scaling properties of the NLS equation. In the small  $\epsilon$  limit, an asymptotic procedure can be used to describe the generation of a family of Peregrine breathers from a modulated plane periodic wave (see [3] for an application to water waves).

The fNLS Equation (7) has the energy law

$$E(T) = E(0) \exp(2\Delta T/\epsilon), \quad E(T) = \int_{-X_L}^{X_L} |Q(T, X)|^2 dX. \tag{9}$$

Here, if  $X = \pm X_L$  in an infinite domain, then  $Q(X, T)$  must decay sufficiently fast at infinity; otherwise in a finite domain periodic boundary conditions are applied at  $X_L$ . The expression (9) can be used to estimate the growth of the wave amplitude as explained in our previous work (see Grimshaw et al. [30]). Briefly, if the absence of forcing the solution is  $Q(X, T : M)$  where  $M$  is a free amplitude parameter, then substitution into (9) yields an estimate for the growth  $M$  under forcing. This is used here as a guide to interpreting each of the cases we consider. If the absence of forcing modulation instability can be measured by the Benjamin–Feir index (BFI), the ratio of wave steepness (nonlinearity) to spectral bandwidth (dispersion) and in the absence of forcing  $BFI \approx 1/\epsilon$  (see Grimshaw and Tovbis [3]). By using the change of variables  $Q = \tilde{Q} \exp(\Delta T/\epsilon)$ , it is readily shown that in the presence of forcing this becomes  $\exp(\Delta T/\epsilon)/\epsilon$ .

The forced NLS Equation (7) is solved numerically on the periodic domain  $-L < x < L$  by using a Fourier spectral method in space and a Runge–Kutta approximation in time. More details can be found in Grimshaw and Maleewong [31] that use a similar approach for numerically solving the forced Koreteweg–de Vries equation. Here we set  $L = 30\text{--}150$  to minimise boundary truncation effects. With this periodic boundary condition, we choose modulation scales so that the solutions decay to the initial background at both ends of the domain well within numerical error. In most cases of the numerical simulations, we set the number of mesh points as 4096 and  $dT = 5 \times 10^{-06}$ , which satisfies numerical stability condition in the Fourier and time domains.

### 3. Numerical Simulations

We consider four cases of initial conditions for the forced NLS Equation (7). Each case represents the generation of solitons and/or breathers.

#### 3.1. Case 1

When  $\Delta = 0$ , the Peregrine breather is given by (see Peregrine [32], Chabchoub and Grimshaw [33])

$$Q(X, T) = M \left[ 1 - \frac{4(1 + 4i\tau)}{1 + 4\chi^2 + 16\tau^2} \right] \exp(2i\tau), \quad \chi = \frac{MX}{\epsilon}, \quad \tau = \frac{M^2 T}{\epsilon}. \tag{10}$$

When  $\Delta \neq 0$ , we solve numerically the forced NLS Equation (7) with the initial condition corresponding to this Peregrine breather (10) at  $T = T_0 < 0$ . With  $\epsilon = 1, M = 1, T_0 = -2, \Delta = 0$  and  $0.2$ , the results are shown in Figures 1–3. The numerical results agree well with the analytical solution over the entire simulation measured by the RMSE of  $|Q|$  in order of  $10^{-7}$ . In the forced case, the amplitude initially grows exponentially at the rate  $2\Delta$  as shown in Figure 3 that agrees with the asymptotic prediction by Grimshaw [18] using the energy law (9) as described above. Note that  $E(T)$  in (9) scales as  $M^2 M^{-1} \epsilon = M \epsilon$  modulo a dependence on  $\tau$ ,

$$E_{PB}(T) = M \epsilon J(\tau), \tag{11}$$

$$J(\tau) = \int_{-\chi_L}^{\chi_L} \left| 1 - \frac{4(1 + 4i\tau)}{1 + 4\chi^2 + 16\tau^2} \right|^2 d\chi.$$

Here  $\chi_L$  is chosen to be sufficiently large so that  $|Q|$  in (10) has decayed to  $M$  there. The function  $J(\tau) \rightarrow 2\chi_L$  as  $\tau \rightarrow \pm\infty$  and has a maximum value at  $\tau = 0$  on a time scale where  $\tau$  is order unity, so that  $T$  is order  $\epsilon M^{-2}$ , much slower than  $\epsilon\Delta^{-1}$  for our parameter choices. In our simulations, the amplitude reaches the first peak around  $T = -0.5$  instead of  $T = 0$  as in the unforced case, and then instead of subsiding to zero as  $T \rightarrow \infty$ , exhibits several oscillations of increasing amplitude, which appear to be the generation of successive Peregrine breathers. The outcome resembles the family of Peregrine breathers to those described in Case 3 below.

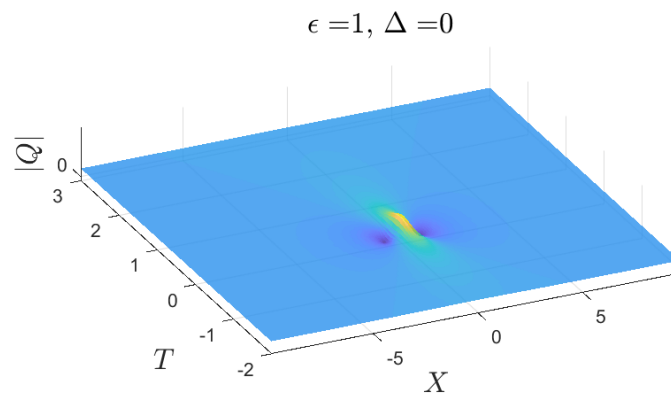


**Figure 1.** Case 1: Surface plot of the unforced Peregrine breather (10) when  $\epsilon = 1.0, M = 1, \Delta = 0.0$ .

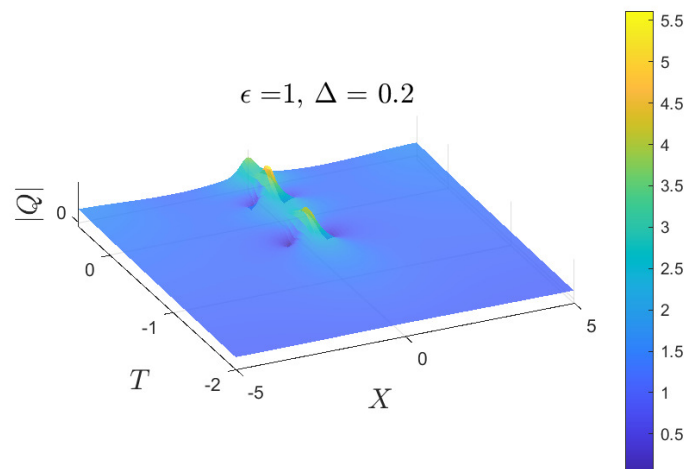


**Figure 2.** Case 1: Surface plot of the forced Peregrine breather when  $\epsilon = 1.0, M = 1, \Delta = 0.2$  with the initial condition (10) at  $T_0 = -2$ .

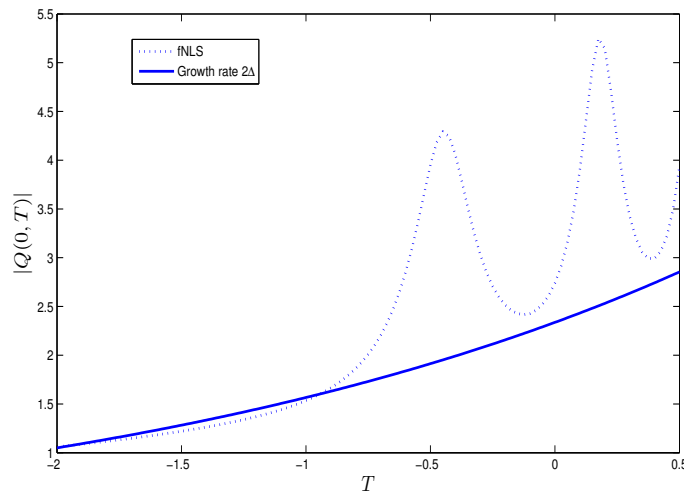


**Figure 3.** Case 1:  $|Q(0, T)|$  when  $\epsilon = 1.0, M = 1, \Delta = 0.2$  with the initial condition that (10) at  $T_0 = -2$ .

3.2. Case 2

When  $\Delta = 0$  there is an exact soliton solution (see Grimshaw [9], Chabchoub and Grimshaw [33]),

$$Q(X, T) = M \operatorname{sech}(\Theta) \exp(i\Phi), \quad \Theta = \Gamma(X - VT), \quad \Phi = \hat{K}X - \Omega T, \quad (12)$$

$$\text{where } \Gamma = \frac{M}{\epsilon}, \quad V = 4\hat{K}, \quad \Omega = \epsilon^2 \hat{K}^2 - \frac{M^2}{\epsilon^2}.$$

The evolution of  $|Q|$  with  $\epsilon = 1, M = 2, \hat{K} = -2$  and  $\Delta = 0$  is shown in Figure 4. The soliton is moving with constant amplitude and speed  $V = 8$  as predicted. With forcing  $\Delta = 0.2$  the evolution of  $|Q|$  with  $\epsilon = 1, M = 2, \hat{K} = -2$  is shown in Figure 5. The soliton is moving with an exponentially increasing amplitude at the rate of  $2\Delta$  as shown in Figure 6. This agrees with the asymptotic prediction of Grimshaw [17] using the energy law (9), while the speed is hardly changed. In the forced case, the amplitude initially grows exponentially at the rate  $2\Delta$  as shown in Figure 3 which agrees with the asymptotic prediction by Grimshaw [18] using the energy law (9) as described above, as here  $E(T) = 2M\epsilon$ . The amplitude of the soliton grows rapidly after  $T > 7$ , and we infer that the solution has become unstable. When the forcing is turned off after  $T > 4$ , the amplitude of the moving soliton is constant.

$$\epsilon = 1.0, \Delta = 0.0$$

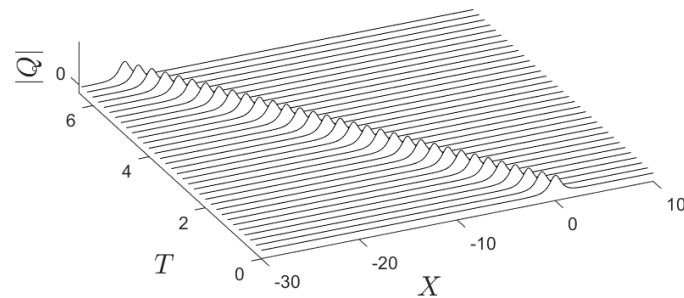


**Figure 4.** Case 2: Constant amplitude moving soliton from Equation (7) when  $\epsilon = 1.0, M = 2, K = -2$ , and  $\Delta = 0.0$ .

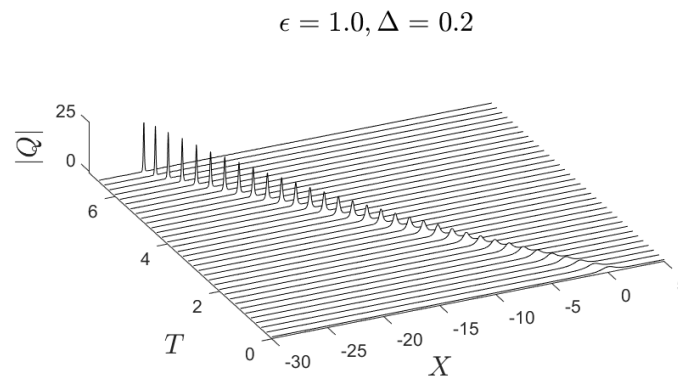


**Figure 5.** Case 2: Growing amplitude moving soliton from Equation (7) when  $\epsilon = 1.0, M = 2, K = -2,$  and  $\Delta = 0.2$ .

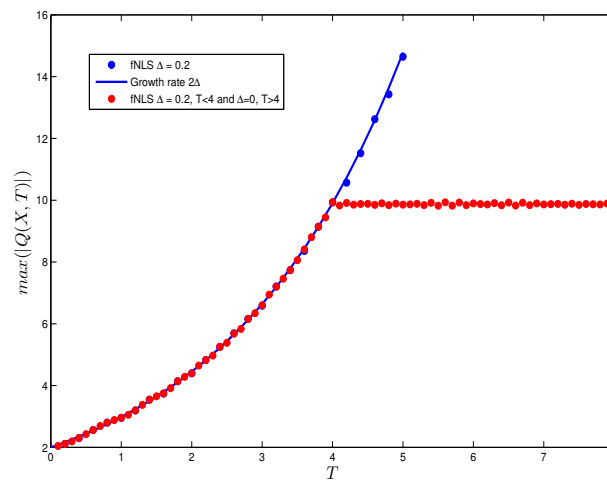


**Figure 6.** Case 2: Maximum of  $|Q(X, T)|$  and growth rate  $2\Delta$  when  $\epsilon = 1.0, M = 2, K = -2,$  and  $\Delta = 0.2,$  forcing is turned off when  $T > 4$ .

### 3.3. Case 3

The initial condition is a slowly varying long wave perturbation:

$$Q(X, 0) = M \operatorname{sech}(\gamma X). \tag{13}$$

Note that we only show cases with  $M = 1,$  as  $M$  can be absorbed into the small parameter  $\delta$  in the derivation of (7), but we did run some simulations for a larger  $M = 2.$  Also  $\gamma$  and  $\epsilon$  are not independent parameters, as rescaling  $\tilde{X} = \gamma X$  is equivalent to replacing  $\epsilon$  by  $\tilde{\epsilon} = \gamma\epsilon$  and then adjusting the time scale  $\tilde{T} = \gamma T.$  Nevertheless, we shall vary both  $\epsilon$  and  $\gamma,$  as well as  $\Delta.$  For small  $\epsilon,$  the dispersion is initially weak and in the absence of forcing the solution evolves into a gradient catastrophe, followed by the generation of a family of Peregrine breathers (see Grimshaw and Tovbis [3]).

#### 3.3.1. Without Forcing ( $\Delta = 0$ )

The outcome for the initial condition (13) when  $\epsilon = 1/33, \gamma = 1, M = 1$  and  $\Delta = 0$  are shown in Figures 7 and 8. There is a gradient catastrophe at  $T = 0.25$  and the generation of a family of Peregrine breathers, in agreement with the theory and numerical predictions described by Grimshaw and Tovbis [3]. The theory predicts that a gradient catastrophe will occur at  $T = 0.25,$  and we see the same result in our numerical simulation as shown in Figure 8. A case (not shown here) with  $\gamma = 1, \epsilon = 1/33$  but with a larger  $M = 2$  was similar. For this larger case of  $M = 2,$  the gradient catastrophe occurs earlier, at approximately  $T = 0.1,$  and this then generates a family of breathers but with less ordered behaviour.

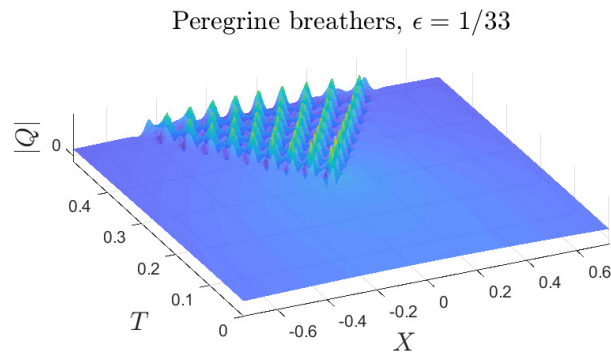


**Figure 7.** Case 3: A family of Peregrine breathers generated from the initial condition (13) when  $\epsilon = 1/33, \gamma = 1, M = 1$  and  $\Delta = 0$ .

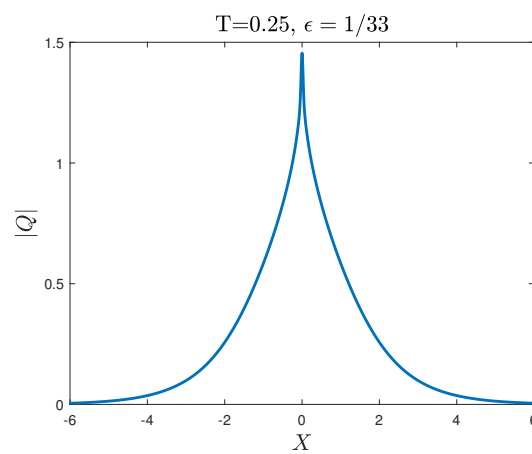


**Figure 8.** Case 3: The gradient catastrophe generated from the initial condition (13) when  $\epsilon = 1/33, \gamma = 1, M = 1$  and  $\Delta = 0$ .

3.3.2. With Forcing ( $\Delta > 0$ )

The forced NLS (7) was solved with the initial condition (13) for various cases with an initial wavenumber  $\gamma = 0.5, 1.0, 2.0, \epsilon = 0.03, 0.1, 0.2, 0.5, 1.0$  and  $\Delta = 0.00, 0.06$ . Note that here  $E(0) = 2M^2/\gamma$  in the energy law (9) where, unlike cases 1 and 2,  $M, \gamma$  are independent parameters and so both the amplitude  $M$  and the wavenumber  $\gamma$  can be affected by the forcing. We show some representative outcomes here.

The case when  $\gamma = 1, \epsilon = 1/33$  and  $\Delta = 0.00, 0.06$  is shown in Figure 9. Without forcing, there is again the initial generation of breathers as shown in Figures 7 and 8, but with the longer time simulation, the breathers combine to form some propagating solitons. As the forcing is increased, the breathers are suppressed, and for  $\Delta = 0.06$  many stationary solitons with growing amplitudes form.

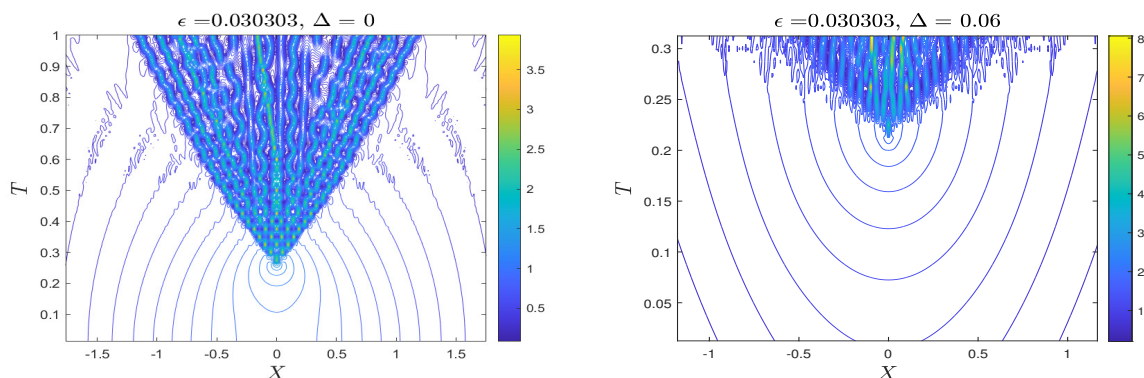


**Figure 9.** Case 3: The initial condition is (13) with  $\gamma = 1.0, \epsilon = 1/33, M = 1$  and  $\Delta = 0, \Delta = 0.06$ .

The case when  $\gamma = 0.5, \epsilon = 0.1$  and  $\Delta = 0.00, 0.06$  is shown in Figure 10. Here  $\tilde{\epsilon} = 0.05$  and is comparable to the case when  $\gamma = 1, \epsilon = 1/33$  as the values of  $\tilde{\epsilon} = 0.05$  and  $\epsilon = 1/33$  are close.

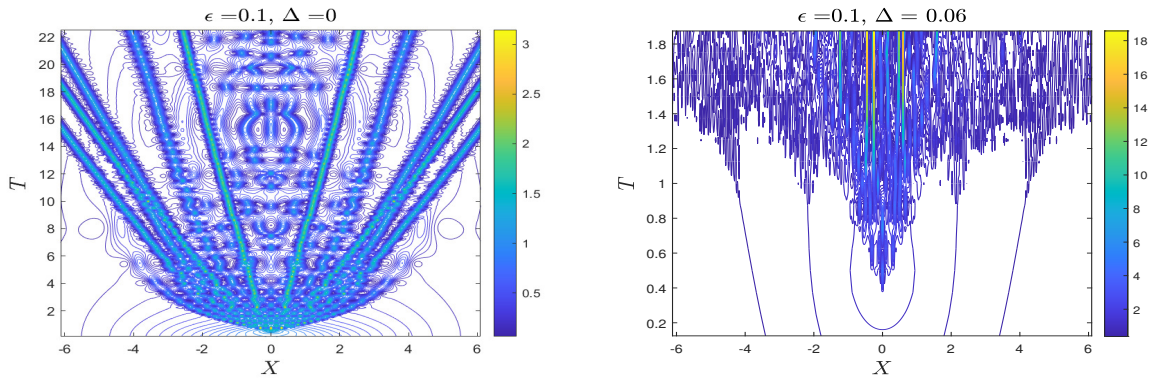


Figure 10. Case 3: The initial condition is (13) with  $\gamma = 0.5, \epsilon = 0.1, M = 1$  and  $\Delta = 0, \Delta = 0.06$ .

The case when  $\gamma = 0.5, \epsilon = 0.2$  and  $\Delta = 0.00, 0.06$  is shown in Figure 11. Here  $\tilde{\epsilon} = 0.1$ , but in comparison with the previous case shown in Figure 10, without forcing there is no sign of the emergence of solitons, and instead a breather family forms and then reforms. However, in the forced simulations, solitons emerge as in the previous case in Figure 10 and as the forcing is increased, there is a transition to just a few stationary solitons with growing amplitudes.

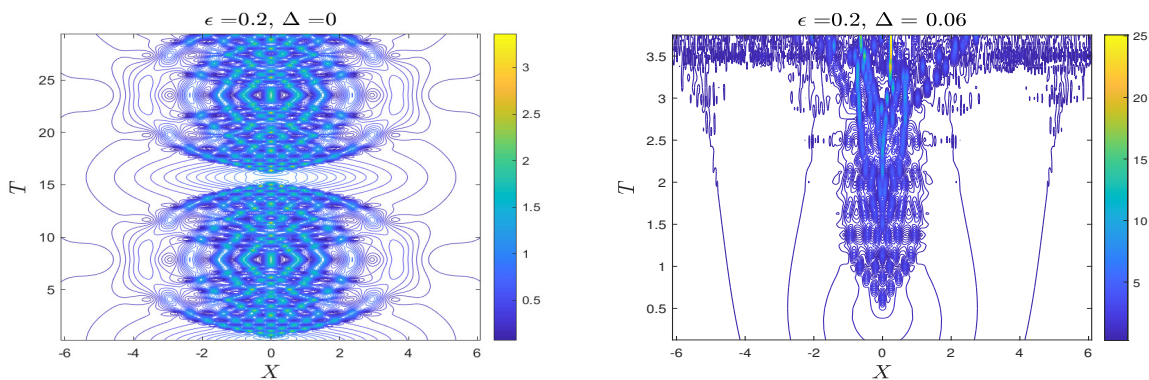


Figure 11. Case 3: The initial condition is (13) with  $\gamma = 0.5, \epsilon = 0.2, M = 1$  and  $\Delta = 0, \Delta = 0.06$ .

The case when  $\gamma = 0.5, \epsilon = 1.0$  and  $\Delta = 0.00, 0.06$  is shown in Figure 12. Here  $\tilde{\epsilon} = 0.5$ , but unlike the two previous cases shown in Figures 10 and 11 when a periodic chain of breathers forms. This case is converted to several growing solitons, now in the forced simulations only a single stationary soliton with a growing amplitude emerges. Plot of the maximum value of  $|Q(X, T)|$  for each  $T$  and  $-L < X < L$  is shown in Figure 13. The amplitude for this forced NLS case grows oscillatory with an overall growth rate  $2\Delta$ . After  $T > 15$  the forcing  $\Delta = 0.06$  is turned off, and the maximum amplitude is shown in Figure 14; it does not increase exponentially but it changes periodically.

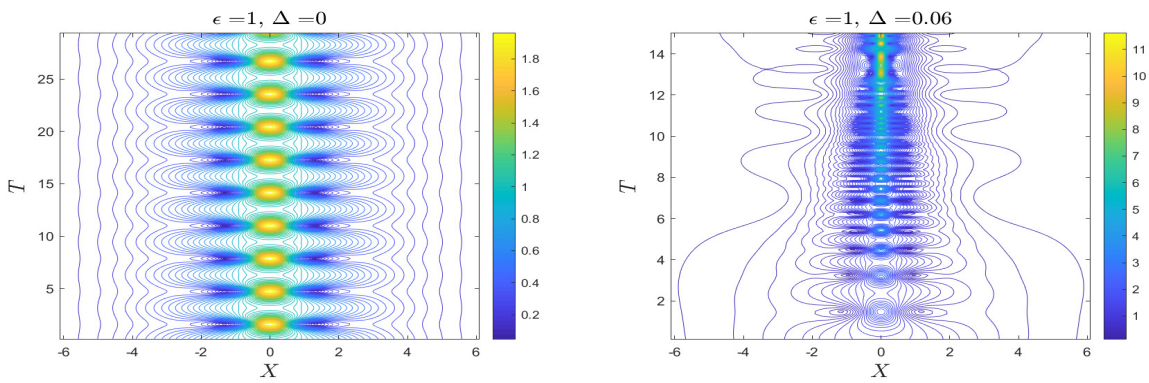


Figure 12. Case 3: The initial condition is (13) with  $\gamma = 0.5, \epsilon = 1.0, M = 1$  and  $\Delta = 0, \Delta = 0.06$ .

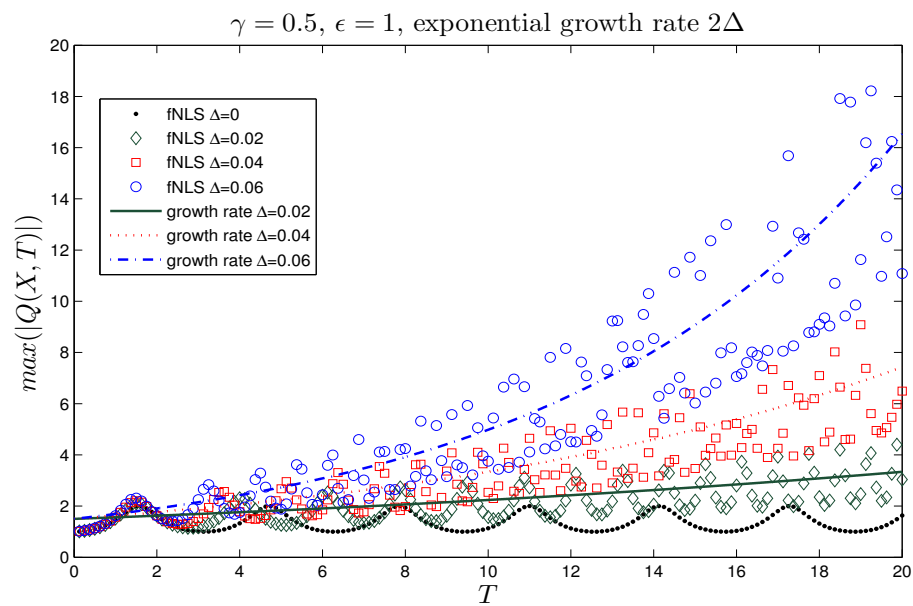


Figure 13. Case 3: Maximum of  $|Q(X, T)|$  and growth rate  $2\Delta$  when  $\gamma = 0.5, \epsilon = 1.0, M = 1$  for various values of  $\Delta$ .

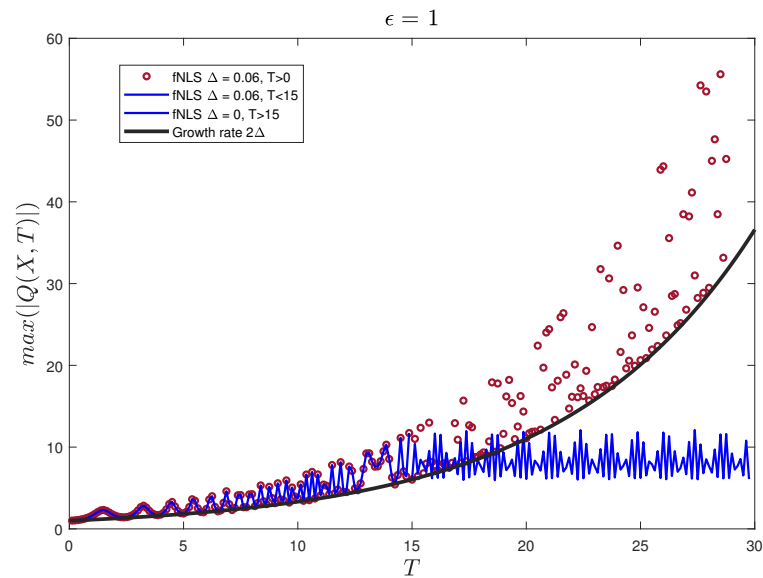


Figure 14. Case 3: Maximum of  $|Q(X, T)|$  and growth rate  $2\Delta$  when  $\gamma = 0.5, \epsilon = 1.0, M = 1$  and  $\Delta = 0.06$ . The forcing is turned off when  $T > 15$ .

The case when  $\gamma = 2.0$ ,  $\epsilon = 0.5$  and  $\Delta = 0.00, 0.06$  is shown in Figure 15. As  $\tilde{\epsilon} = 1.0$ , this is equivalent to Case 2, and indeed only a single stationary soliton forms, with a growing amplitude at exactly the predicted exponential rate of  $2\Delta$ , see Grimshaw [17].

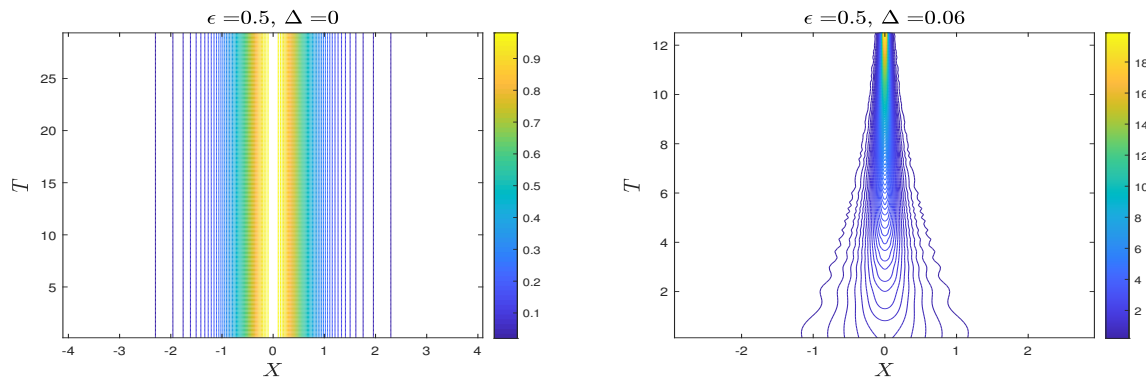


Figure 15. Case 3: The initial condition is (13) with  $\gamma = 2.0$ ,  $\epsilon = 0.5$ ,  $M = 1$  and  $\Delta = 0, \Delta = 0.06$ .

The case when  $\gamma = 2.0$ ,  $\epsilon = 1.0$  and  $\Delta = 0.00, 0.06$  is shown in Figure 16. Here  $\tilde{\epsilon} = 2.0$  is larger and a different picture emerges, looking more like the modulation instability cases shown in Case 4 below. There is evidence of the formation of both breathers and solitons with amplitudes increasing.

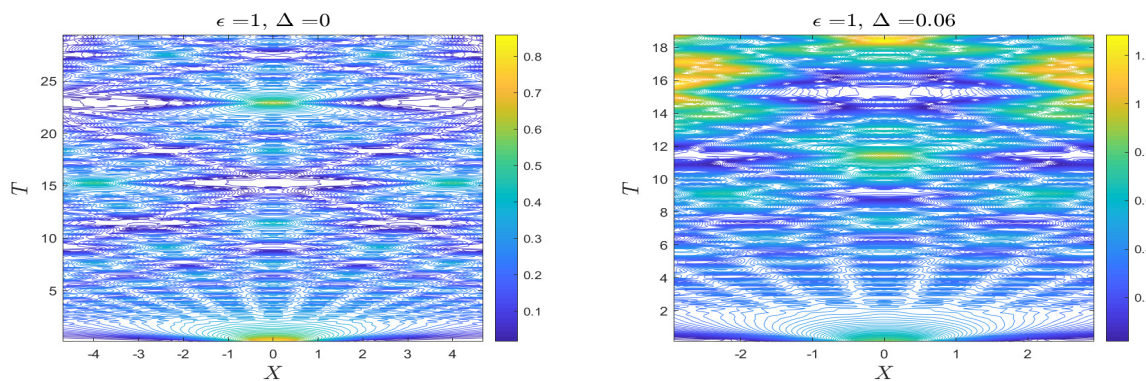


Figure 16. Case 3: The initial condition is (13) with  $\gamma = 2.0$ ,  $\epsilon = 1.0$ ,  $M = 1$  and  $\Delta = 0, \Delta = 0.06$ .

### 3.4. Case 4

The initial condition is a long-wave periodic perturbation with wavenumber  $K$ ,

$$Q(X, 0) = M(1 + \alpha \cos KX), \tag{14}$$

where  $0 < \alpha \ll 1$ . When  $\Delta = 0$  there is modulation instability for  $\epsilon K < \sqrt{2}|M|$ , and maximum growth when  $\epsilon K = \sqrt{1/2}|M|$ . We fix  $\alpha = 0.1$  and show some representative simulations varying  $M$ ,  $K$ , and  $\Delta$ . With this initial condition (14) where the initial amplitude does not decay at the boundaries, the computational domain  $L$  is set large enough and given by a multiple of  $2\pi/K$  to prevent some spurious effects from the boundaries. Because we have applied a periodic boundary condition in the Fourier spectral method, some waves will appear to come from the boundaries in this case.

### 3.4.1. Without Forcing ( $\Delta = 0$ )

We examined the case when  $M = 0.1$ ,  $\epsilon = 1/33$  and  $K = 0.1$ . This parameter setting is at the long-wave end of the modulation instability regime, and the outcome is a family of Peregrine breathers very similar to that shown in Case (3) in Figure 7. Cases when  $M = 1$ ,  $\epsilon = 1$ ,  $K = \sqrt{0.1}$  and  $M = 1$ ,  $\epsilon = 1$ ,  $K = \sqrt{0.5}$  were also investigated. Both these cases are within the modulation instability regime, and we found the generation of breathers as has been demonstrated in many works (see for instance Osborne [2]). The case  $M = 1$ ,  $\epsilon = 1$ ,  $K = 4$  is formally outside the modulation instability regime. Nevertheless a periodic breather chain develops after  $T = 18$  with amplitudes less than 3 (see Figure 17).

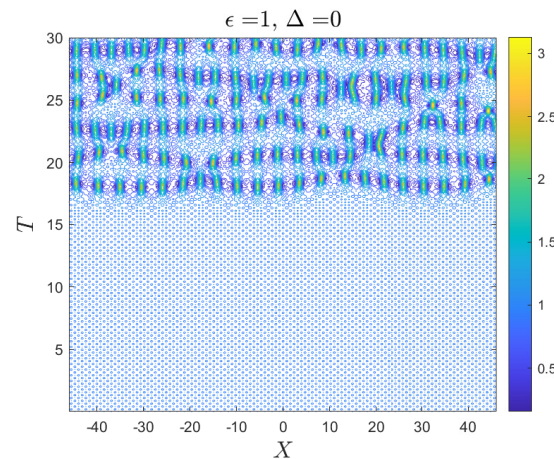
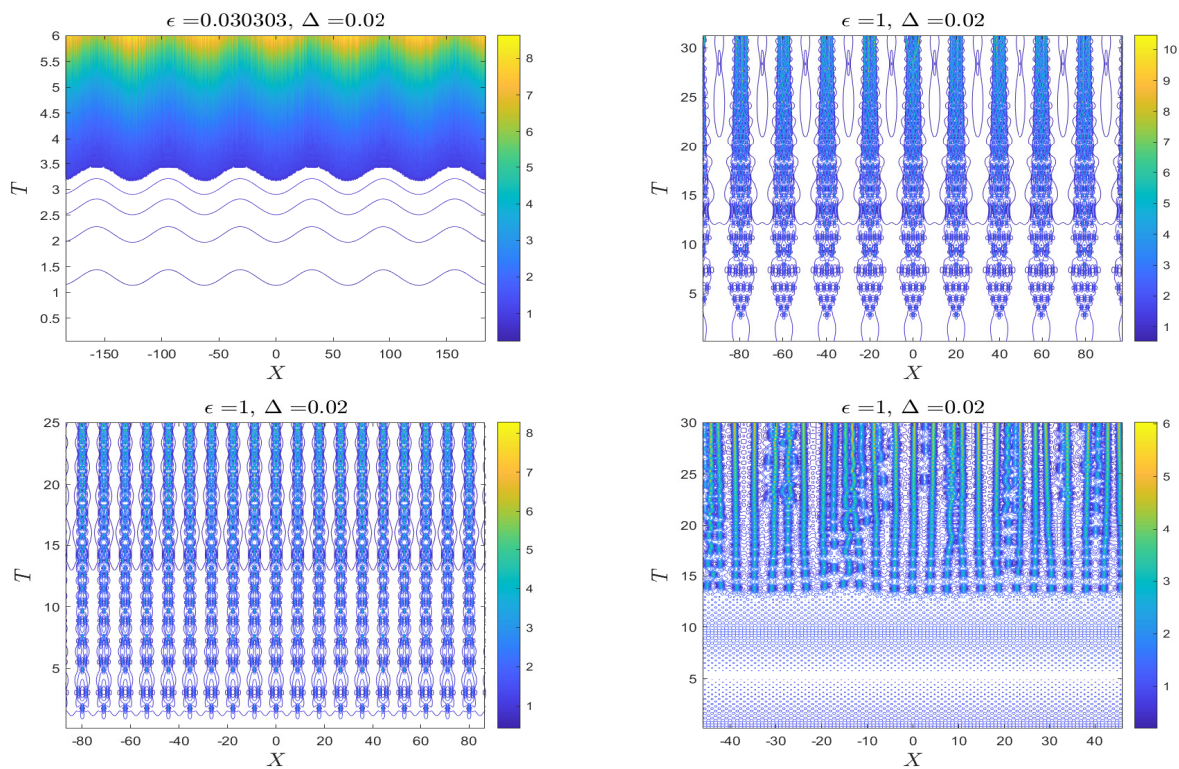


Figure 17. Case 4: The initial condition is (14) with  $\epsilon = 1.0$ ,  $M = 1$ ,  $K = 4$  and  $\Delta = 0$ .

### 3.4.2. With Forcing ( $\Delta > 0$ )

The case when  $M = 0.1$ ,  $\epsilon = 1/33$ ,  $K = 0.1$  and  $\Delta = 0.02$  is shown in Figure 18. As the forcing is increased, the family of Peregrine breathers is converted to many stationary solitons with amplitudes increasing in time and with a short length scale. The cases when  $M = 1.0$ ,  $\epsilon = 1.0$ ,  $K = \sqrt{0.1}$ , and  $\Delta = 0.02$  is shown in Figure 18 (top right) and the case of  $M = 1.0$ ,  $\epsilon = 1.0$ ,  $K = \sqrt{0.5}$  with  $\Delta = 0.02$  is shown in Figure 18 (bottom left). Plots of the maximum amplitude versus time  $T$  when  $K = \sqrt{0.1}$  for various values of  $\Delta$  is shown in Figure 19. The amplitudes grow with the exponential growth rate  $2\Delta$ . The case when  $M = 1.0$ ,  $\epsilon = 1.0$ ,  $K = 4$ , and  $\Delta = 0.02$  is shown in Figure 18 (bottom-right). In all these cases as the forcing is increased the breathers are eliminated and progressively fewer solitons are formed with growing amplitudes. Plots of the maximum amplitude versus time  $T$  for various values of  $\Delta$  is shown in Figure 20, the amplitudes grow with the exponential growth rate  $2\Delta$ . The maximum amplitude does not grow at the early time steps, as a certain time interval is required for the excitation of the wave amplitude. For the unforced case, when the maximum amplitude grows to its maximum average, it does not grow further. The higher the value of the forcing amplitude, the smaller the time interval required for the excitation. The number and trajectories of these solitons appears to depend quite sensitively on the parameter settings. When the forcing is turned off after  $T > 15$  s, the contour plot of the soliton formed is shown in Figure 21 (left). The trains of solitons (large waves) interact with each other. Because there is no forcing after  $T > 15$  s, the maximum amplitude does not grow. It maintains the mean value which is approximately equal to the final amplitude at  $T = 15$ , as shown in Figure 21 (right).



**Figure 18.** Case 4: The initial condition is (14) with  $\Delta = 0.02$ . Contour plots of  $|Q|$  when  $M = 0.1$ ,  $\epsilon = 1/33, K = 0.1$  (top left),  $M = 1, \epsilon = 1, K = \sqrt{0.1}$  (top right),  $M = 1, \epsilon = 1, K = \sqrt{0.5}$  (bottom left), and  $M = 1, \epsilon = 1, K = 4$  (bottom right).

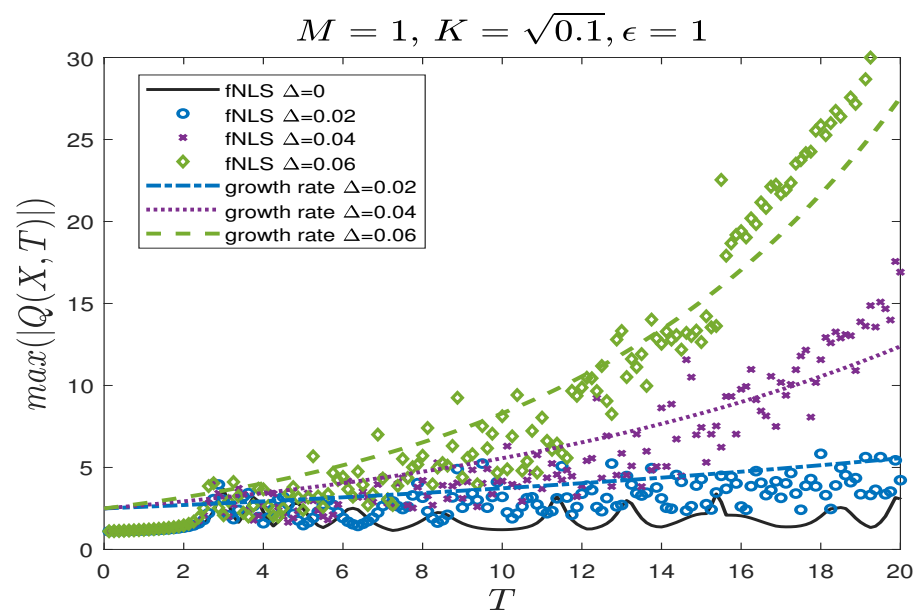


**Figure 19.** Case 4: The initial condition is (14). Maximum of  $|Q(X, T)|$  and growth rate  $2\Delta$  when  $M = 1.0, \epsilon = 1.0, K = \sqrt{0.1}$  for various values of  $\Delta$ .

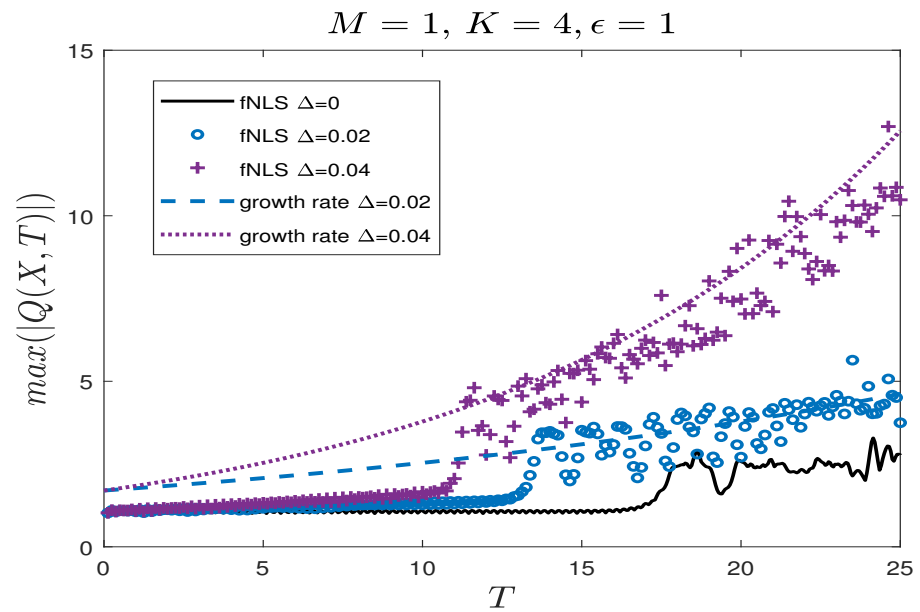


**Figure 20.** Case 4: The initial condition is (14). Maximum of  $|Q(X, T)|$  and growth rate  $2\Delta$  when  $M = 1.0, \epsilon = 1.0, K = 4.0$  for various values of  $\Delta$ .

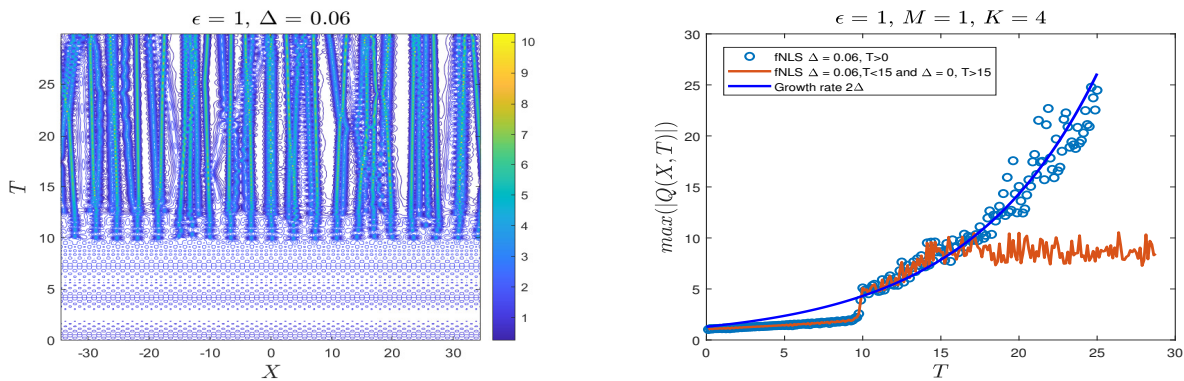


**Figure 21.** Case 4: The initial condition is (14). Contour plot and the maximum of  $|Q(X, T)|$  with growth rate  $2\Delta$  when  $M = 1.0, \epsilon = 1.0, K = 4.0$  for  $\Delta = 0.06$ . Forcing is turned off when  $T > 15$ .

### 3.5. Initial Random Noise

In this section, we investigate the effect of initial random noise on the growth rate of the wave amplitude for each case presented in the previous sections. We impose random noise at the initial time step and investigate the dynamics of breathers, solitons, and modulation instability. The initial random noise is set by

$$Q(X, T_0) + M_R \cdot \text{Rand}, \tag{15}$$

where  $Q(X, T_0)$  is the initial condition as above when there is no random noise. Rand is a complex random number where the real and imaginary parts are uniformly distributed values ranged over  $[0, 1]$ . Random noise is inserted on every grid point for  $-20 < X < 20$  and the value of Rand is zero outside this region.  $M_R$  is the magnitude of the random noise. We set  $M_R = 0.1$  for case 1 and  $M_R = 0.5$  for cases 2–4. It is approximately 25% of the initial amplitude. We numerically investigate how this initial random noise affects the growth rate under forcing. The results for each case are shown as follows.

**Case 1:** The effect of initial random noise on the Peregrine breather is shown in Figure 22 with  $\Delta = 0.2$ ,  $\epsilon = 1$ , and  $M = 1$ . It can be compared to the case without initial noise shown in Figure 2. The main feature of breathers can still be seen in Figure 22 (left). The maximum amplitude over the entire domain is shown in Figure 22 (right) and is comparable with the theoretical growth rate  $2\Delta$ . The initial random noise again affects the increment of maximum amplitude earlier than  $T = 0$ , as before when  $-0.5 < T$ . The position of these large amplitude waves remains relatively stationary.

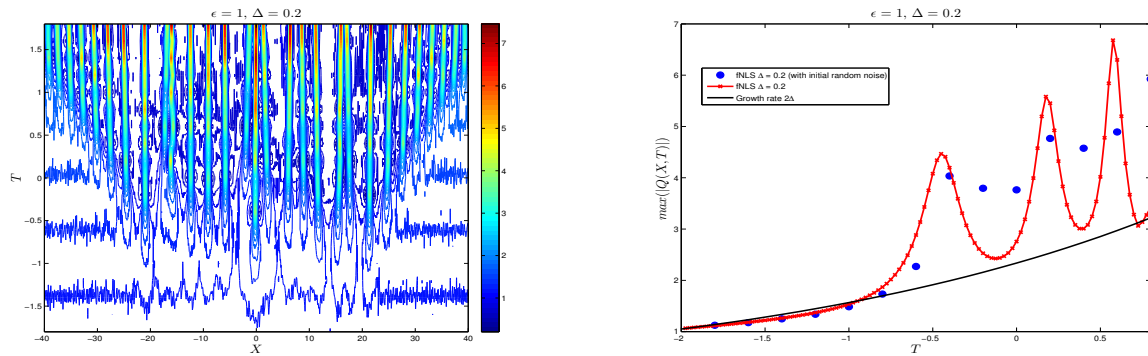


**Figure 22.** Initial random noise, Case 1: Contour plot of  $|Q|$  when  $\Delta = 0.2$  (left) and the maximum of  $|Q(X, T)|$  with the predicted growth rate  $2\Delta$  (right).

**Case 2:** The evolution of a moving soliton with initial random noise is shown in Figure 23 (left). Here  $\epsilon = 1$ ,  $M = 2$ ,  $K = -2$ , and  $\Delta = 0.2$ . This result can be compared with the case without initial noise, as shown in Figure 5. The soliton is moving with an exponentially increasing amplitude by the growth rate  $2\Delta$ . The plot of the maximum amplitude is shown in Figure 23 (right). Unlike case 1, the maximum amplitude grows monotonically. The results with and without initial random noise are similar except that now two stationary solitons are generated downstream while the leading soliton travels with the theoretical speed upstream. We infer that initial random noise that has a large enough amplitude can generate some new stationary soliton waves.

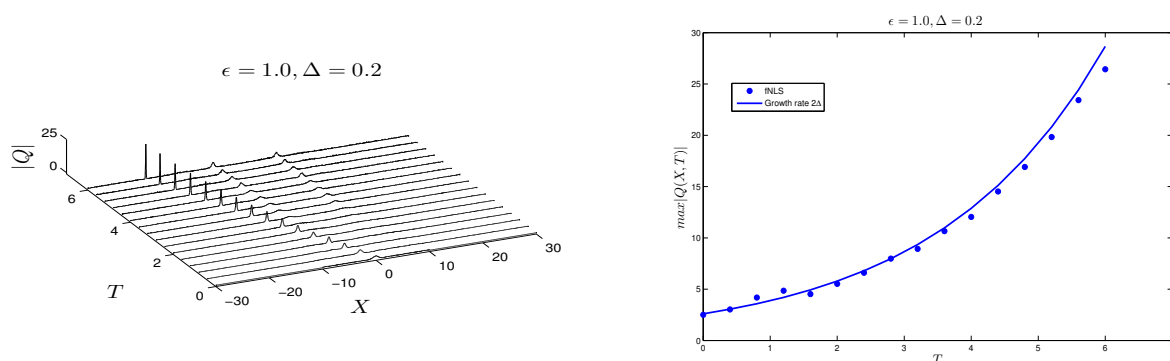


**Figure 23.** Initial random noise, Case 2: Evolution of  $|Q|$  when  $\epsilon = 1$ ,  $M = 2$ ,  $K = -2$  and  $\Delta = 0.2$  (left) and the maximum of  $|Q(X, T)|$  with the predicted growth rate  $2\Delta$  (right).

**Case 3:** In the absence of forcing and initial random noise, a periodic chain of breathers forms. The location of the breathers is stationary along  $X = 0$  as shown in Figure 12. The result with initial random noise is shown in Figure 24 (left). In this simulation initial random noise shifts the location of the periodic chain of breathers slightly to  $X < 0$ , with the same of order of amplitude and with an indication of a second chain forming in  $X > 0$ . For a forcing case with  $\Delta = 0.06$ , the maximum amplitude is increased, see Figure 24 (right), with the mean growth rate  $2\Delta$ , see Figure 25.

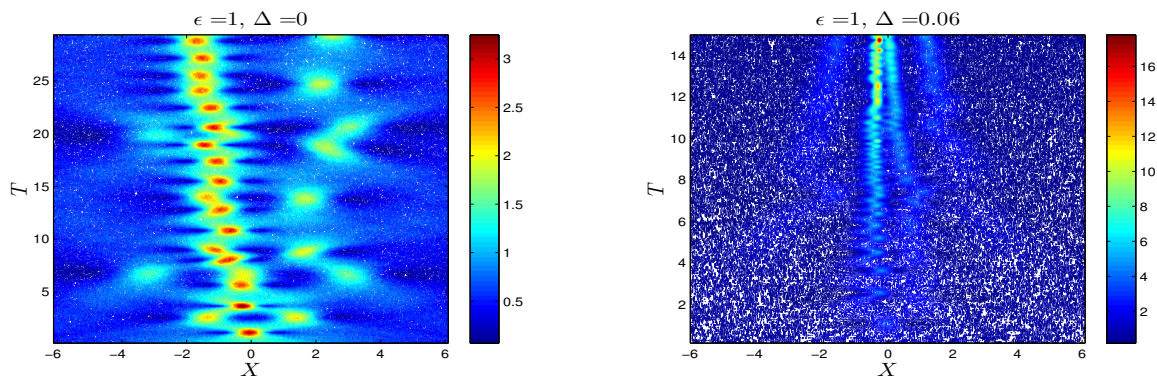


**Figure 24.** Initial random noise, Case 3: Contour plots of  $|Q|$  when  $\Delta = 0$  (left) and  $\Delta = 0.06$  (right).

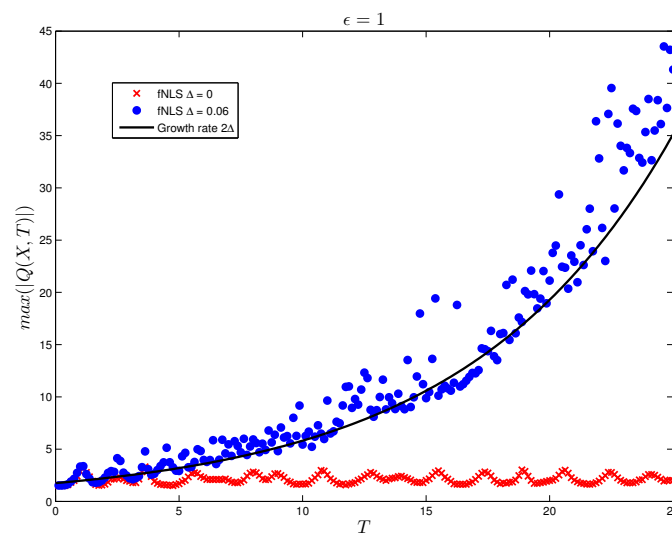


**Figure 25.** Initial random noise, Case 3: The maximum of  $|Q(X, T)|$  with the predicted growth rate  $2\Delta$  when  $\gamma = 0.5$ ,  $\epsilon = 1.0$ , and  $\Delta = 0.06$ .

**Case 4:** The results with initial random noise are shown in Figure 26 for  $M = 1$ ,  $\epsilon = 1$ ,  $K = 4$ , and  $\Delta = 0, 0.04$ . There is no modulation instability in this case. In the absence of forcing (see Figure 26 (left)), periodic plane waves are generated. Initial random noise perturbs the pattern of these waves while the maximum amplitude over the entire domain is preserved. In contrast, for the forcing case, the maximum amplitude is increased with a mean growth rate  $2\Delta$  (see Figure 26 (right)). Compared with the case without initial random noise in Figure 20, when  $\Delta = 0.04$  the maximum amplitude grows but requires a certain time interval for wave growth. Initial random noise stimulates the maximum growth rate to be earlier with the robust growth rate  $2\Delta$ . Instead of increasing  $K$ , we fixed  $K = 4$  and increased  $\epsilon$ . We found that for  $\epsilon = 4$  the time  $T_1 \approx 70$  for the amplitude to be stimulated but finite, which is much larger than  $T_1$  for the case of smaller  $\epsilon = 1$ .

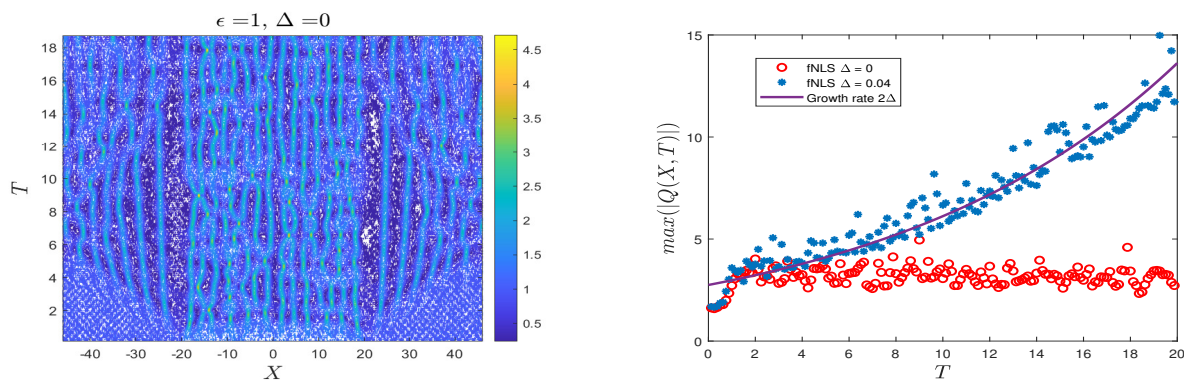


**Figure 26.** Initial random noise, Case 4: Contour plots of  $|Q|$  when  $\Delta = 0$  (left) and the maximum of  $|Q(X, T)|$  with the predicted growth rate  $2\Delta$  (right) when  $M = 1$ ,  $\epsilon = 1.0$  and  $K = 4$ .

#### 4. Discussion and Summary

In this paper, motivated by an application to wind waves, we have used the forced NLS Equation (7) expressed in canonical form to model the generation of wave packets and breathers by adding a linear growth term to the usual NLS equation. In the absence of such forcing, the principal solutions of the NLS equation are solitons and breathers, representing wave packets and possibly rogue waves (see Kharif et al. [1], Osborne [2], Grimshaw and Tovbis [3] for instance). In the forced NLS equation, the forcing is represented by a linear growth term with a rate parameter  $\Delta$  so that  $\Delta > 0$  and  $\Delta = 0$  represents cases with and without forcing respectively (see Leblanc [11], Touboul et al. [12], Montalvo et al. [13], Brunetti et al. [14], Slunyaev et al. [15], Grimshaw [16] for the context of the generation of water waves by wind). In this context, the non-dimensional growth rate parameter  $\Delta$  depends on several physical factors, especially the wind shear, the surface roughness, and the initial water wave wavelength. It can range from  $O(10^{-2})$  for weak winds to  $O(10)$  for strong winds (see Leblanc [11], Touboul et al. [12], Slunyaev et al. [15] for instance). Here we have varied  $\Delta$  over the range from zero to order unity, covering the range of weak to moderate forcing appropriate for our weakly nonlinear model.

Four scenarios are investigated through an appropriate choice of initial condition. These scenarios are (1) an initial condition which in the unforced case would generate a Peregrine breather (10); (2) an initial condition which in the unforced case would generate a moving soliton (12); (3) a slowly varying long wave perturbation which in the unforced case would generate either a few solitons for  $\epsilon$  of order unity, or a family of Peregrine breathers when  $\epsilon$  becomes very small; (4) a long-wave periodic perturbation which in the unforced case would generate modulation instability and the formation of both solitons and breathers.

In case 1, a Peregrine breather is formed when  $\Delta = 0$  and agrees with the well-known exact solution. When  $\Delta > 0$ , a forced Peregrine breather initially develops with an increased amplitude, growing at twice the linear growth rate, but instead of decreasing to zero, the amplitude continues to grow and oscillates with increasing frequency. In case 2, with  $\Delta = 0$  a steadily moving soliton with a constant amplitude forms. When  $\Delta > 0$ , the soliton amplitude grows at the rate  $2\Delta$ , twice the linear growth rate while continuing to move with a constant speed. In case 3, with  $\Delta = 0$  and with a very small dispersion parameter  $\epsilon = 1/33$ , there is a gradient catastrophe followed by the formation of a family of Peregrine breathers as expected (see Grimshaw and Tovbis [3]). When  $\Delta > 0$ , in contrast to the unforced case the Peregrine breathers are replaced by a mixture of breathers and solitons. Three scenarios were found, the generation of mainly moving solitons with increasing amplitudes, nearly stationary solitons with increasing amplitude, and a combination of both breathers and increasing amplitude solitons. In case 4, a periodic long-wave perturbation with wavenumber  $K$  is imposed as the initial condition. Modulation instability with wavenumber  $K$  occurs when  $\epsilon K < \sqrt{2}|M|$  where  $M$  is the initial amplitude of the periodic long wave. When  $\Delta = 0$ , a mixture of solitons and breathers form as is well-known

(see Osborne [2] for instance). However, as the forcing parameter  $\Delta$  increases, the breathers begin to be eliminated and are replaced by solitons with growing amplitudes, progressively fewer forming as the forcing increases.

For each case (1–4) of these initial conditions, we investigated the effect of initial random noise. The case of an initial moving soliton is unchanged except that some small solitons are generated downstream ( $X > 0$ ) due to the initial random noise perturbation. The maximum growth rate  $2\Delta$  can still be used to make an accurate prediction of the amplitude growth. For cases when breathers form, initial random noise shifts the locations of the unforced solutions. When forcing is involved, the maximum growth rate of the breathers increases and oscillates with a mean growth rate  $2\Delta$ . For the case of an initial periodic plane wave, initial random noise changes the modulation pattern from deterministic to chaotic with the implication that the location of the maximum amplitude cannot be determined exactly. However, the growth of the maximum amplitude is still approximately  $2\Delta$ . Overall, the predicted growth rate  $2\Delta$  is robust for these initial value problems with and without an initial random noise effect.

Modulation instability and the subsequent formation of small amplitude waves that generate large amplitude waves or sometimes rogue waves has been studied experimentally for water waves by many authors (see for instance [28]). This large wave is generally unstable due to its growing nonlinear wave packet amplitude when the Benjamin–Feir index (BFI) increases. In this ocean application, large-amplitude waves are generally unstable due to the growing nonlinear wave packet amplitude and modulation instability, measured by the BFI, the ratio of wave steepness (nonlinearity) to spectral bandwidth (dispersion). In this work,  $\text{BFI} \approx 1/\epsilon$  (see Grimshaw and Tovbis [3]). Even for  $\text{BFI} = 1$  which is a moderate value, external forcing that can be viewed as wind blowing over the sea causes modulation instability, and large-amplitude waves are developed. For instance, see Figures 18 for initial periodic plane wave with wind effects  $\Delta = 0.02$ . When there is a wind effect  $\Delta > 0$ , we characterise the development of large-amplitude waves into two stages: the first stage is the development of breathers which could be interpreted as a random sea state as time evolves, and then a second stage forms with large-amplitude waves. The large waves in the second stage collect energy from neighbouring small waves with different wave frequencies. Rogue waves are observed when the BFI is large with amplitudes three or four times the background sea state during their evolution (see for instance [2,28]). In our present work for  $\text{BFI} = 1$  modulation instability occurs in the predicted long-wave perturbation range ( $\epsilon K < 2|M|$ ) in the first stage, but then large amplitude waves develop due to the wind effect. The larger the value of the wind forcing coefficient, the larger are the waves in the second stage, and they become unstable. Instead of using the periodic wave plane as an initial condition, in case (3) the initial condition of a slowly varying long wave perturbation with a sech-profile also develops into a modulation instability region.

Recent work by [29] shows the region of high and low wave frequency nonlinear wave interaction where a nonlinear wave component can grow exponentially, leading to rogue wave packets. Outside this region, the small waves are stable. This situation is comparable with our results shown in Figure 11 with and without wind effects. It can be seen from the case without wind effect that a sequence of breathers is generated, but introducing a wind effect can generate large waves growing in wave amplitude and stationary. An explicit formula that expresses rogue wave formation under wind effect and nonlinear wave packet interaction remains a challenge for further studies.

**Author Contributions:** The authors contributed equally to this work. Conceptualization, methodology, software, validation, formal analysis, investigation, resources, data curation, writing—original draft preparation, writing—review and editing, visualization, supervision, project administration by M.M and R.H.J.G. All authors have read and agreed to the published version of the manuscript

**Funding:** RG was supported by the Leverhulme Trust through the award of a Leverhulme Emeritus Fellowship EM-2019-030.

**Acknowledgments:** RG was supported by the Leverhulme Trust through the award of a Leverhulme Emeritus Fellowship EM-2019-030. This research was partially supported by International SciKU Branding (ISB), Faculty of Science, Kasetsart University, Bangkok, Thailand.

**Conflicts of Interest:** The authors declare no conflict of interest.

## References

1. Kharif, C.; Pelinovsky, E.; Slunyaev, A. *Rogue Waves in the Ocean*; Advances in Geophysical and Environmental Mechanics and Mathematics; Springer: Berlin/Heidelberg, Germany, 2009.
2. Osborne, A.R. Nonlinear Ocean Waves and the Inverse Scattering Transform. In *Scattering*, 1st ed.; Academic Press: Cambridge, MA, USA, 2010.
3. Grimshaw, R.; Tovbis, A. Rogue waves: Analytical predictions. *Proc. Royal Soc.* **2013**, *469*, 20130094. [[CrossRef](#)]
4. Grimshaw, R.; Pelinovsky, E.; Talipova, T.; Sergeeva, A. Rogue internal waves in the ocean: Long wave model. *Eur. Physical J. Special Topics* **2010**, *185*, 195–208. [[CrossRef](#)]
5. Chow, K.W.; Chan, H.N.; Grimshaw, R.H. Modulation instability of internal waves in a smoothly stratified shallow fluid with a constant buoyancy frequency. *Nat. Hazards Earth Syst. Sci. Brief Comm.* **2019**, *19*, 583–587. [[CrossRef](#)]
6. Benney, D.J.; Newell, A.C. The propagation of nonlinear wave envelopes. *J. Math. Phys.* **1967**, *46*, 133–139. [[CrossRef](#)]
7. Zakharov, V.E. Stability of periodic waves of finite amplitude on the surface of a deep fluid. *J. Appl. Mech. Tech. Phys.* **1968**, *9*, 190–194. [[CrossRef](#)]
8. Hasimoto, H.; Ono, H. Nonlinear modulation of gravity waves. *J. Phys. Soc. Japan* **1972**, *33*, 805–811. [[CrossRef](#)]
9. Grimshaw, R. Envelope solitary waves. In *Solitary waves in Fluids: Advances in Fluid Mechanics*; Grimshaw, R., Ed.; WIT Press: Southampton, UK, 2007; Volume 45, pp. 159–179.
10. Akhmediev, N.; Pelinovsky, E. Discussion and Debate: Rogue Waves-Towards a Unifying Concept? *Eur. Physical J. Special Topics* **2010**, *185*, 1–266. [[CrossRef](#)]
11. Leblanc, S. Amplification of nonlinear surface waves by wind. *Phys. Fluids* **2007**, *19*, 101705. [[CrossRef](#)]
12. Touboul, J.; Kharif, C.; Pelinovsky, E.; Giovanangeli, J.P. On the interaction of wind and steep gravity wave groups using Miles' and Jeffreys' mechanisms. *Nonlin. Proc. Geophys.* **2008**, *15*, 1023–1031. [[CrossRef](#)]
13. Montalvo, P.; Kraenkel, R.; Manna, M.A.; Kharif, C. Wind-wave amplification mechanisms: possible models for steep wave events in finite depth. *Nat. Hazards Earth Syst. Sci.* **2013**, *13*, 2805–2813. [[CrossRef](#)]
14. Brunetti, M.; Marchiando, N.; Berti, N.; Kasparian, J. Nonlinear fast growth of water waves under wind forcing. *Phys. Lett. A* **2014**, *378*, 1025–1030. [[CrossRef](#)]
15. Slunyaev, A.; Sergeeva, A.; Pelinovsky, E. Wave amplification in the framework of forced nonlinear Schrödinger equation: The rogue wave context. *Phys. D* **2015**, *301*, 18–27. [[CrossRef](#)]
16. Grimshaw, R. Generation of wave groups. In *IUTAM Symposium Wind Waves*; Grimshaw, R.; Hunt, J., Johnson, E., Eds.; Elsevier IUTAM Procedia Series; Elsevier: Amsterdam, The Netherlands, 2018; Volume 26, pp. 99–101.
17. Grimshaw, R. Generation of wave groups by shear layer instability. *Fluids* **2019**, *4*, 39. [[CrossRef](#)]
18. Grimshaw, R. Two-dimensional modulation instability of wind waves. *J. Ocean. Eng. Mar. Energy* **2019**, *5*, 413–417. [[CrossRef](#)]
19. Miles, J.W. On the generation of surface waves by shear flows. *J. Fluid Mech.* **1957**, *3*, 185–204. [[CrossRef](#)]
20. Miles, J.W. Surface wave generation revisited. *J. Fluid Mech.* **1993**, *256*, 427–441. [[CrossRef](#)]
21. Morland, L.C.; Saffman, P.G. Effect of wind profile on the instability of wind blowing over water. *J. Fluid Mech.* **1993**, *252*, 383–398. [[CrossRef](#)]
22. Janssen, P. *The Interaction of Ocean Waves and Wind*; Cambridge University Press: Cambridge, UK, 2004.
23. Stiassnie, M.; Agnon, Y.; Janssen, P.A.E.M. Temporal and spatial growth of wind waves. *J. Phys. Ocean.* **2007**, *37*, 106–114. [[CrossRef](#)]
24. Sajjadi, S.G.; Hunt, J.C.R.; Drullion, F. Asymptotic multi-layer analysis of wind over unsteady monochromatic surface waves. *J. Eng. Maths* **2014**, *84*, 73–85. [[CrossRef](#)]
25. Zakharov, V.E.; Resio, D.; Pushkarev, A. Balanced source terms for wave generation within the Hasselmann equation. *Nonlin. Proc. Geophys.* **2017**, *24*, 581–597. [[CrossRef](#)]
26. Chabchoub, A.; Hoffmann, N.; Akhmediev, N. Rogue wave observation in a water wave tank. *Phys. Rev. Lett.* **2011**, *106*, 204502. [[CrossRef](#)] [[PubMed](#)]
27. Chabchoub, A.; Slunyaev, A.; Hoffmann, N.; Dias, F.; Kibler, B.; Genty, G.; Dudley, J.M.; Akhmediev, N. The Peregrine breather on the zero-background limit as the two-Soliton degenerate solution: An experimental study. *Front. Phys.* **2021**, *9*, 633549. [[CrossRef](#)]
28. Onorato, M.; Osborne, A.R.; Serio, M. Modulational instability and non-Gaussian statistics in experimental random water-wave trains. *Phys. Fluids* **2005**, *17*, 078101. [[CrossRef](#)]
29. León, S.P.; Osborne, A.R. Role of nonlinear four-wave interactions source term on the spectral shape. *J. Mar. Sci. Eng.* **2020**, *8*, 251. [[CrossRef](#)]
30. Grimshaw, R.; Hunt, J.; Johnson, E. Preface. In *IUTAM Symposium Wind Waves*; Grimshaw, R., Hunt, J., Johnson, E., Eds.; Elsevier: Amsterdam, The Netherlands, 2018; Volume 26, pp. 1–2.

31. Grimshaw, R.H.J.; Maleewong, M. Transcritical flow over two obstacles: Forced Korteweg de Vries framework. *J. Fluid Mech.* **2016**, *809*, 918–940. [[CrossRef](#)]
32. Peregrine, D.H. Water waves, nonlinear Schrödinger equations, and their solutions. *J. Aust. Math. Soc. Series B* **1983**, *25*, 16–43. [[CrossRef](#)]
33. Chabchoub, A.; Grimshaw, R. The hydrodynamic nonlinear Schrödinger equation: Space and time. *Fluids* **2016**, *1*, 23–32. [[CrossRef](#)]